LUNDS UNIVERSITET

Department of Psychology

Visual Cognition Alterations in Central Visual Impairment: A Multiple Case Study on Adolescents

Author Maria Barbara Smorczewska
Master's Thesis Master of Science in Psychology
Year 2

Supervisor: Finn Lennartsson, Johannes Björkstrand

Abstract

This multiple case-study investigated cerebral visual impairment (CVI) by comparing patients to age-matched controls using a multimodal framework: a Swedish-adapted Dutton's Questionnaire, OCT (GCL+ thickness), visual field perimetry, and 7T fMRI pRF mapping. I evaluated whether V1 pRF expansion relates to retinal degeneration and dorsal versus ventral behavioral deficits. Results revealed structure–function dissociations: macular ganglion cell thinning lacked spatial concordance with perimetric deficits, while pRF expansion accompanied dual-stream visual impairments. These findings demonstrate that neuroplastic adaptations shape CVI phenotypes semi-independently of retino-structural damage, emphasizing the necessity of multimodal evaluation for improved diagnostics and rehabilitation.

Keywords: Population Receptive Fields, Central Visual Impairment, Perception, Two-Stream Hypothesis, Optical Coherence Tomography, Visual Field

Thank You!

For the countless hours spent last year in the hospital lab: thank you so much, Rio and Finn (my supervisor), for your patience, your ideas, and your willingness to help even on very short notice! To my other supervisor, Johannes: thank you so much for your advice and expertise. To Hanna Maria: thank you for being so kind and willing to teach a student outside of the medical faculty during short breaks between patients. To Kabilan, Karin, and Kalle: thank you for being so generous with your time. To Dereje and Hugo: it was a pleasure to share the lab with you. I would also like to thank Prof. Maciej Burzyk, whose dedication and passion for teaching is the reason I pursued the biological path. Finally, I want to thank my hardworking parents for making this life accessible to me, my friends and family for visiting me from every corner of the world, my little sister for always standing by my side, and my dear roommate Alicia for helping me create a space where I could study and learn.

Introduction

Cerebral visual impairment

Injury to the brain has become the most common cause of visual impairment in children in the developed world, and can lead to cerebral visual impairment (CVI), which includes symptoms such as subnormal visual acuity, cognitive visual problems, eye-movement disorders and visual field defects (Mitry et al., 2013). It is a brain-based disorder of visual function, which can include both lower-order functions (e.g. edge detection) as well as higher-level functions (e.g. facial recognition)(Chang et al., 2024). Most commonly, CVI presents clinically as a neurodevelopmental disorder, following an injury to visual pathways and visual processing areas during fetal development, birth, or early infancy (Ospina, 2009). As humans rely heavily on visual perception during early development (Tierney & Nelson, 2009) the neurodevelopmentally disruptive nature of CVI may adversely affect visual development itself, while also influencing the development of other functions that rely on visual information (Chang et al., 2024). This can include spatial orientation, cognitive functioning, motor coordination, and psychosocial skills (Chang et al., 2024).

Ventral and Dorsal Stream Impairments in CVI

Dual-stream processing hypothesis refers to the concept, firstly presented by Goodale & Milner, (1992) and Mishkin et al., (1983) that there exist two separate pathways of visual processing: the dorsal "where" stream and the ventral "what" stream. Both processing streams project from primary visual cortex (V1), with dorsal stream projecting towards the motor cortex through parieto-occipital areas, and ventral stream projecting to inferior temporal lobes (Goodale & Milner, 1992; Mishkin et al., 1983). This process is illustrated in Figure 1. Visual information is processed in parallel within the streams, with dorsal stream primarily processing information regarding spatial location (e.g. spatially guided motor movements) and ventral stream primarily processing information related to recognition and memory such as shape and object recognition (Goodale & Milner, 1992; Mishkin et al., 1983). Importantly, despite cross-interaction between the streams, they are anatomically and functionally distinct to the point that selective impairment is possible (Pamir et al., 2024).

In case of CVI, current research points towards the dorsal stream being at bigger risk of functional damage, which is referred to as dorsal stream vulnerability (DSV) (Bennett et al., 2020). Behavioral observation data shows, that children diagnosed with CVI often exhibit more problems with tasks associated with dorsal "where" processing such as locating objects in space, judging distances, or perceiving objects in motion (Dutton et al., 2006; Fazzi et al., 2009; Goodale & Milner, 1992; McKillop & Dutton, 2008, 2008). In children born preterm, the frequently observed vulnerability of dorsal-stream visual functions may partly reflect the characteristic distribution of white-matter injury of prematurity which typically affects the posterior periventricular white matter that is particularly susceptible to injury during this

developmental period (Volpe et al., 2011). Injury in these regions may affect posterior optic radiation and occipito-parietal connections, providing a potential anatomical basis for the higher prevalence of dorsal-stream dysfunction reported in children born preterm (Dutton, 2009). It is important to note that CVI patients can also present, to a varying degree, with impairments in the ventral "what" stream, however those impairments however, rarely occur in isolation contrary to the DSV, and are usually comorbid with dorsal stream impairments (Macintyre-Beon et al., 2010).

Figure 1.

The Dorsal and Ventral Visual Processing Streams

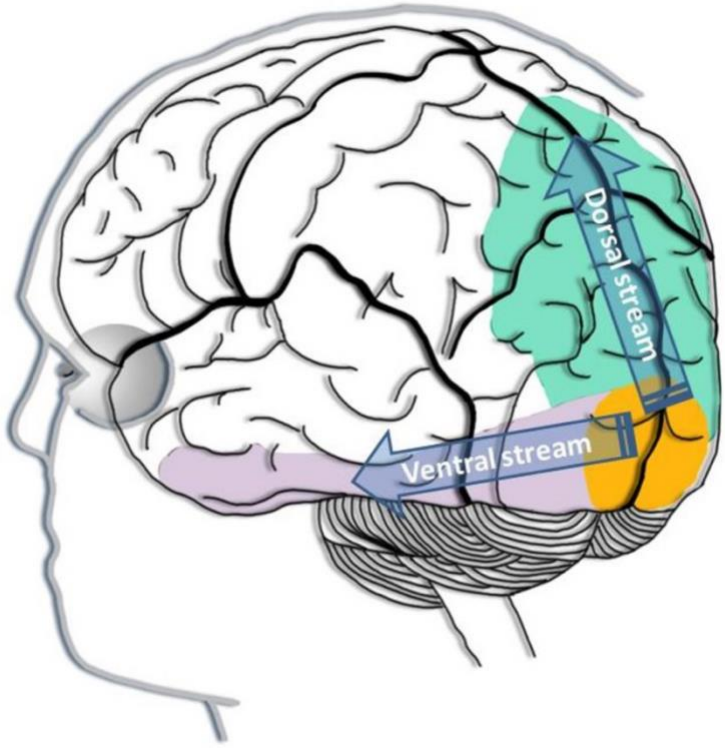

Note. From *Ventral-dorsal streams*, by Selket, 2007, Wikimedia Commons (https://commons.wikimedia.org/wiki/File:Ventral-dorsal_streams.svg), licensed under CC BY-SA 3.0.

Multimodal Diagnostic Approaches in CVI

Behavioral Profiling: Dutton's Questionnaire and Visual Stream Functioning

Clinical evaluations of CVI require analyzing how visual deficits manifest in every-day behavior (Dutton, 2009; Philip & Dutton, 2014; Sakki et al., 2021). The Dutton's CVI Questionnaire (further referred to as "Dutton's Questionnaire") is a clinical inventory designed to capture higher-order perceptual and functional visual deficits in children with CVI (Dutton, 2011; Dutton et al., 2006). Because standard ocular and visual acuity examinations frequently fail to detect brain-based visual processing impairments, Dutton's questionnaire utilizes inventory items to map everyday functional difficulties onto neuroanatomical models

of visual processing (Dutton et al., 2006). From a psychometric standpoint, Dutton's questionnaire was not designed as a standardized diagnostic or screening instrument with normative cutoffs or a validated quantitative scoring scale (*Cerebral Visual Impairment Assessment*, 2023) Instead, it functions as a qualitative and quasi-quantitative inventory of synthesized, commonly reported visual and perceptual impairments associated with CVI (Dutton, 2009; Macintyre-Beon et al., 2012).

The items in the existing Swedish adaptation of Dutton's questionnaire used in this study, target the most ecologically representative visual challenges reported in CVI while maintaining balance across the dual-stream processing pathways (Goodale & Milner, 1992; Kravitz et al., 2013). Rather than evaluating isolated visual tasks under laboratory conditions, the items focus on everyday behaviors that map onto visual streams: dorsal-predominant subscale targets behaviors dependent on occipito-parietal processing, including egocentric spatial mapping, visual search, and visually guided movement (e.g., "orientation at home", "judging distances and height differences") (Dutton, 2009; Bennett et al., 2020); ventral-predominant subscale target behaviors dependent on occipito-temporal processing, including feature integration, allocentric representations[1], and object identification (e.g., "Recognizing people's faces", "Identifying objects on a carpet") (Dutton, 2009, 2011; Ospina, 2009).

Importantly, assessing visual function through everyday behavioral inventories requires acknowledging that real-world tasks are multidetermined (Dutton, 2011; McDowell, 2023). Everyday visual performance is conditioned not only on visual stream processing integrity, but also on interacting higher-order cognitive networks (Kooiker et al., 2016; Kravitz et al., 2013). For example, navigating a home or locating an object in a cluttered room demands dorsal stream spatial processing alongside top-down executive function, sustained attention control, and visual working memory (Chokron & Dutton, 2016, 2016; Kooiker et al., 2016). Consequently, reported inventory impairments reflect the combined, perceptual load and cognitive effort required to compensate for underlying visual pathway degradation. (Chokron & Dutton, 2016; Kooiker et al., 2016; McKillop & Dutton, 2008).

Structural and Retinal Biomarkers: Optical Coherence Tomography

In CVI, early damage to the immature retro-geniculate visual pathway can initiate secondary Retrograde Trans-Synaptic Degeneration (RTSD) along the primary visual pathway (Dinkin, 2017). Lesions within the optic radiation interrupt retinal outflow signaling, causing secondary trans-neuronal degeneration that travels through the lateral geniculate nucleus (LGN) and induces apoptosis[2] of retinal ganglion cell bodies (Dinkin, 2017). Consequently, degradation in central white matter alters the structural

[1] Mental representations of spatial information that encode the location of objects or places relative to one another, rather than relative to the observer's own position or orientation.

[2] A regulated form of programmed cell death in which cells undergo controlled self-destruction through coordinated molecular processes, typically without inducing substantial inflammation in surrounding tissue.

integrity of the retina, providing a physical footprint of retro-geniculate damage in CVI (Lennartsson et al., 2021).

Measurements of RTSD, which can be informative in CVI diagnosis, are obtained by Optical Coherence Tomography (OCT) which provides a non-invasive, quantitative measurement of the inner retinal layers, with the possibility to analyze the ganglion cell-inner plexiform layer (GCL+) thickness specifically in the retina. (Lennartsson et al., 2021), illustrated in Figure 2. While OCT isolates structural cell loss within the retina, visual field perimeter complements these structural measurements by mapping their functional consequences across visual field (VF). In CVI patients, localized patterns of GCL+ thinning seem to correspond to the spatial distribution of retro-geniculate damage as well as deficits in the VF function (Lennartsson et al., 2018). This marker allows clinicians and researchers to confirm that the visual loss is underpinned by permanent loss of retro geniculate afferent fibers rather than an ocular pathology (Lennartsson et al., 2018, 2021)

Together, quantifying GCL+ structural integrity via OCT and functional VF loss via visual field perimetry can establish the baseline, bottom-up signal summation reaching the V1 (Keller et al., 2014). In CVI research, disentangling this primary sensory loss (subcortical tract damage and secondary RGCL apoptosis) from central cortical visual dysfunction (higher-order stream processing deficits) has important, methodological advantages (Chang et al., 2024; Dinkin, 2017; Lennartsson et al., 2018, 2021). Establishing a structural and perimetric baseline ensures that behavioral impairments captured by Dutton's questionnaire and cortical alterations observed via functional MRI are accurately interpreted relative to the strength and spatial distribution of the incoming sensory signal.

Figure 2.

Illustration of Retinal Ganglion Cell Layer

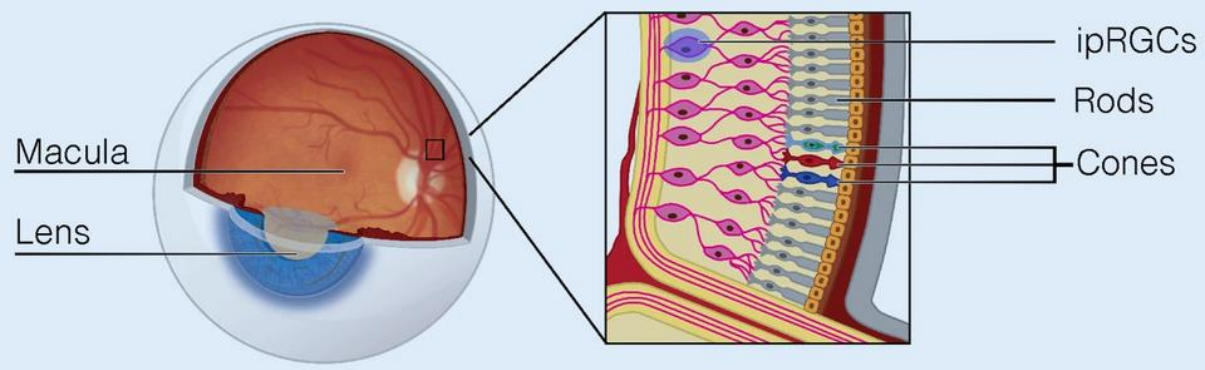

Reproduced from *Overview of the retina photoreceptors (a)*, by C. Blume, C. Garbazza, and M. Spitschan, 2019, Wikimedia Commons. CC BY 4.0.

Note. *Intrinsically photosensitive Retinal Ganglion Cells* (*ipRGCs are melanopsin-containing retinal neurons that directly sense ambient light to regulate non-visual processes, primarily circadian rhythms and the pupillary light reflex.*

Population Receptive Field Mapping and Cortical Reorganization in CVI

Population receptive field (pRF) mapping via functional magnetic resonance imaging (fMRI) quantifies the functional organization, spatial resolution, and regional connectivity of the human visual cortex by modeling voxel-wise responses to moving stimulus apertures. (Dumoulin & Wandell, 2008; Elul & Levin, 2024; Haak et al., 2012). Key pRF parameters include visual field position, being the preferred location of the receptive field center, and pRF size, which reflects the spatial extent over which a cortical population integrates visual information (Dumoulin & Wandell, 2008). These properties are modulated by network-level interactions, attentional state, and contextual input, making pRF parameters a dynamic reflection of cortical organization and reorganization, rather than a static, anatomical property (Haak et al., 2012; Elul & Levin, 2024).

At the sensory level, pRF size dictates spatial frequency processing: smaller pRFs meaning pooling smaller amounts of neurons at a more localized area) process higher spatial frequencies allowing for high acuity vision, whereas larger pRFs integrate low spatial frequencies to support coarse spatial processing and global scene integration (Elul & Levin, 2024). Naturally, foveal pRFs grow proportionally to the increased eccentricity, with the smallest, most compact pRFs being naturally in the fovea, with larger pRFs being found in the visual periphery (Haak et al., 2012) Consequently, the behavioral impact of altered pRF properties depends on retinotopic location. Pathological, foveal pRF expansion may lower spatial resolution, degrade spatial tuning and induce visual crowding that aligns with ventral pathway deficits, such as impaired face recognition (Elul & Levin, 2024). Conversely, peripheral pRF alterations may disrupt global visual integration and spatial processing, contributing to dorsal-stream dysfunction (Elul & Levin, 2024).

In CVI, structural MRI commonly identifies injuries to posterior visual pathways, yet these anatomical metrics often fail to fully explain the severity of functional deficits and specific alterations of vision (Bennett et al., 2020; Fazzi et al., 2009; Good et al., 1994). Functional MRI demonstrates altered recruitment, activation, and connectivity across visual pathways, particularly within the dorsal stream during visuospatial tasks, suggesting post-lesion cortical reorganization (Bennett et al., 2020; Pamir et al., 2024). Incorporating pRF mapping into CVI diagnostic protocols may be a way to capture these physiological correlates of neuroplasticity (Martín et al., 2016). By moving beyond static structural damage to map alterations in spatial tuning, pRF analysis can help explain higher-order perceptual phenomena, such as motion processing impairments and spatial crowding (Bennett et al., 2020; Elul & Levin, 2024; Pamir et al., 2024). However, whether these pRF alterations reflect compensatory adaptation or maladaptive neuroplasticity in CVI remains unresolved (Elul & Levin, 2024).

Mechanics of Structural-Functional Reorganization of Visual Processing

Cortical Plasticity vs. Peripheral Degeneration

In CVI, early damage to retro-geniculate pathways disrupts the development of retinotopic organization, raising fundamental questions regarding the nature and extent of subsequent cortical adaptation. (Bennett et al., 2020; Lennartsson et al., 2021; Martín et al., 2016). The possibility of developmental decoupling suggests that central cortical reorganization may operate partly independently of peripheral cell loss (Elul & Levin, 2024). Importantly, because optical input and photoreceptor density remain intact, the primary peripheral bottleneck stems from reduced GCL+ density resulting from RTSD (Lennartsson et al., 2018). This reduction in incoming signals forces a neurodevelopmental trade-off: cortical visual areas cannot simultaneously maintain fine spatial acuity (which requires small, densely packed pRFs) and complete visual field coverage (Elul & Levin, 2024). Within this adaptive framework, potential pRF expansion represents a cortical mechanism that prioritizes visual field coverage over spatial resolution, enlarging receptive field sizes to maintain a continuous, coherent retinotopic map across visual space (Elul & Levin, 2024). Consequently, surviving cortical populations integrate visual signals over broader spatial extents, explaining both decreased perimetric visual field sensitivity and the decoupling of central functional architecture from the exact extent of peripheral structural damage (Elul & Levin, 2024; Haak et al., 2012).

Functional Trade-off in Neurodevelopmental Plasticity

In typical visual development, a neural pathway from the retina through the lateral geniculate nucleus (LGN) to the V1 establishes coherent, spatial mapping, which preserves a layout of the visual field by integrating information from both eyes (Ribeiro et al., 2025). In CVI, however, early injury to posterior visual pathways disrupts the standard neuroplastic development (Martín et al., 2016; Ospina, 2009).This plastic reorganization introduces a critical functional trade-off between the requirements of the ventral and dorsal streams (Pamir et al., 2024). If neuroplastic mechanisms prioritize high spatial resolution, small, but more interconnected pRFs are being preserved in the fovea (Gomez et al., 2018). However, if peripheral pRFs also remain small or abnormally contracted, the cortex may lose the capacity for large-scale spatial pooling needed across global VF locations (Elul & Levin, 2024). This creates a local processing bias and leads to "islands of vision" separated by unintegrated visual space (Cooper & O'Sullivan, 2016; Elul & Levin, 2024). While the high, visual acuity within these isolated islands is preserved, they lack a continuous spatial map, possibly resulting in dorsal stream deficits in navigation, obstacle avoidance, and visually guided movement (Cooper & O'Sullivan, 2016; Martín et al., 2016). The opposite adaptive strategy includes expanding pRF sizes, particularly in the visual periphery. Enlarged pRFs allow for broader spatial pooling of injury-surviving neuronal populations, reconstruction of maximally continuous spatial map, mitigating the impairments in dorsal pathway processing (Cooper & O'Sullivan, 2016; Martín et al., 2016).

Among the CVI patients, the second adaptive strategy (pRFs expansion) seems to be more prevalent (Martín et al., 2016). The natural vulnerability of the occipito-parietal brain regions to the early-life injuries (Goodale & Milner, 1992; Mishkin et al., 1983) and resulting DSV (Bennett et al., 2020) appears to trigger the compensatory plasticity, prioritizing global visual integration over preservation of high, focal resolution (Elul & Levin, 2024; Martín et al., 2016). While the spatial continuity is preserved through the higher level of peripheral-foveal integration, the sheer foveal acuity reduces, resulting in potential increase in the clinical, ventral stream-related symptoms, while expected dorsal stream-related symptoms may be mitigated (Elul & Levin, 2024; Martín et al., 2016).

The Present Study

Synthesis and Research Gap

Recent advancements in research regarding clinical presentation of CVI yielded many new insights into both behavioral and structural changes that are associated with this disorder. Importantly, it shed light onto the characteristics of the physical and psychological adaptations that may be at play among CVI patients. Optical coherence tomography quantifies axonal loss via measure of GCL+ thinning resulting from retrograde trans-synaptic degeneration following subcortical and optic radiation injury while perimetric VF mapping allows for tracking the optical consequences of that degeneration (Dinkin, 2017; Keller et al., 2014; Lennartsson et al., 2018, 2021; Volpe et al., 2011). Concurrently, the advancements in fMRI with pRF population receptive field modeling allow to isolate central cortical spatial tuning across retinotopic visual areas (Elul & Levin, 2024; Gomez et al., 2018; Haak et al., 2012). At the behavioral level, structured clinical inventories, such as Dutton's CVI Questionnaire, capture everyday higher-order visual difficulties across dorsal and ventral processing streams in hope to pinpoint possibly most specific areas of impairment. (Bennett et al., 2020; Dutton, 2009, 2011; Macintyre-Beon et al., 2010).

Despite these advancements within individual modalities, little is known regarding the dynamics between the modalities. To my knowledge, no single study to date has integrated OCT structural biomarkers, perimetric visual fields, pRF computational mapping, and behavioral inventories within a unified clinical profile in CVI. Consequently, it remains unknown how peripheral retinal degeneration topographically relates to central pRF, how dual-stream behavioral profiles map onto primary neurostructural damage, and whether computational cortical adaptation serves as a potential compensatory mechanism that reshapes clinical presentation, or merely as a persisting, pathological consequence of neural injury (Chang et al., 2024; McDowell, 2023; Pamir et al., 2024).

This study addresses these gaps through a multimodal framework designed to model visual information processing in CVI and aims at pinpointing the interdependence of different modalities which are affected by this disorder. Mapping dual-stream functional asymmetries on Dutton's Questionnaire to establish whether CVI presents with a dorsal dominance and whether cortical pRF expansion relates to

overall behavioral deficit load. Evaluating whether structural, computational, and behavioral metrics converge into a shared CVI patient profile.

To evaluate this multimodal framework, I addressed the following research questions and hypotheses.**;** Does regional retinal structural loss relates to cortical spatial neuroplasticity (pRF size,σ) across early visual areas in CVI? I hypothesized that among the participants regional retinal thinning across visual field eccentricities will relate to enlarged cortical pRF sizes in early visual areas (V1-V3) Dinkin, 2017; Keller et al., 2014; Lennartsson et al., 2018, 2021), reflecting altered cortical spatial tuning (Elul & Levin, 2024; 2018; Haak et al., 2012). Regarding the behavioral pattern among the CVI participants, I proposed the following research question: Do individuals with CVI display a dorsal-dominant pattern of visual dysfunction, and does expand cortical spatial tuning (pRF size) correlate with overall behavioral visual impairment? I predicted that the dominant pattern among the participants will be associated with the dorsal stream impairments compared to ventral impairments as measured via the Dutton's questionnaire (Bennett et al., 2020; Dutton, 2009, 2011; Fazzi et al., 2009; Macintyre-Beon et al., 2010). I also predicted that enlarged pRFs size will be associated with more overall impairments noted in the questionnaire (Elul & Levin, 2024; Pamir et al., 2024). The last research question concerns the clinical and cognitive presentation of the CVI: Do structural (OCT), computational (pRF), and behavioral metrics converge to demonstrate a developmental structure–function dissociation in CVI? I predicted that extensive structural brain damage without pRF expansion will predict global impairments across both visual streams with a slight dorsal-dominant bias (Volpe et al., 2011); conversely, enlarged pRFs will mitigate structural loss by selectively reducing dorsal impairments, resulting in lower-than-expected dorsal deficits and relatively greater ventral impairments relative to primary structural damage severity (Elul & Levin, 2024; Pamir et al., 2024).

Methods

Study Design

In this thesis I chose a retrospective embedded multiple-case design (Yin, 2018). I decided to implement this methodological approach due to the large individual variation between the study participants and significant portion of missing data among the fMRI scans. The primary case is defined as a patient-control dyad, allowing for the comparison of behavioral, structural, and functional patterns of visual performance. Within each dyad, three units of analysis are examined: (1) behavioral performance via the Swedish adaptation of Dutton's Questionnaire, (2) structural retinal integrity via OCT, and (3) functional cortical activity in pRFs and structural evaluation via fMRI. Due to the retrospective nature of the data and clinical realities, a two-tiered analysis strategy was implemented to handle missing data and individual variation with preserving as many data points as possible. Tier 1 consisted of cross-case analysis. Each

dyad was included in the primary behavioral and structural analysis. Cross-case synthesis juxtaposed Dutton Questionnaire profiles with OCT structural metrics, and MRI to map behavioral-structural phenotypes. Tier 2 focused on nested, functional sub-analysis: Due to artifacts or missing fMRI data, a nested subset of only two fMRI-complete dyads was selected for full functional imaging analysis. The simplified model of this research design framework can be seen in Figure 3.

The analysis proceeded from the specific to the general. First, I conducted within-case analysis for each dyad across all three modalities. Second, I looked at a cross-case synthesis for the behavioral and structural dimensions across the full cohort. Finally, I looked at cross-case synthesis of specifically the functional visual cortex impairment for the two, complete cases, to nuance the behavioral-structural patterns observed in Tier 1. In terms of measurement method, I chose a mixed-methods design**.** I selected this approach because understanding the clinical manifestation of CVI requires the integration of both qualitative behavioral data and quantitative physiological and structural data. While the overall analytical framework is designed as a qualitative case-study (focusing on pattern matching and within-case synthesis of individual dyads), the embedded units of analysis include both qualitative components (behavioral profiles from Dutton's Questionnaire) and quantitative components (metrics from OCT scans and functional imaging data from fMRI). I chose this design as it preserves individual heterogeneity and focuses on maximally detailed description of observable CVI presentations across parallel clinical modalities, rather than inferring causal relationships between brain function and behavior.

Figure 3.

Research Design Framework

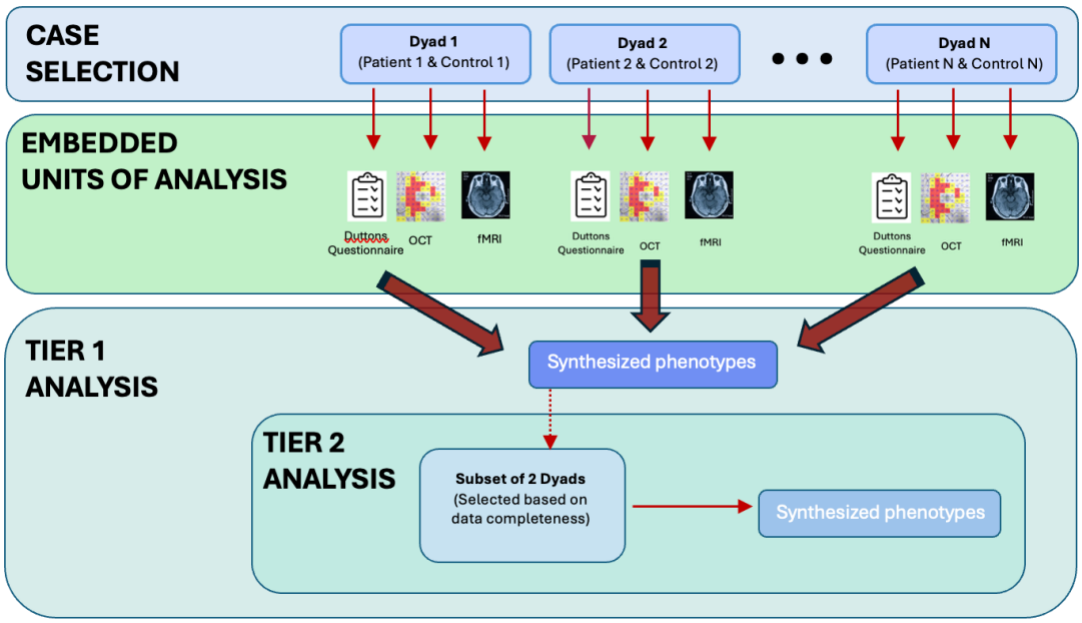

Participants

Clinical participants were recruited from the regional registry of individuals medically diagnosed with CVI across the Skåne region, Sweden. Study supervisors screened patient medical records to select candidates with CVI acquired prenatally or in early infancy. To ensure candidates could comply with study procedures, such as completing behavioral questionnaires and maintaining head stability during MRI and OCT scanning, screening excluded individuals with comorbid neurological or psychiatric conditions, severe visual impairment, or advanced intellectual or behavioral impairments. Eligible candidates were then contacted, creating an initial cohort of 15 participants. All participants and controls were 15 years of age during the period of data collection. Following one dropout after the first session, 14 participants completed the full study protocol (4 females, 10 males). However, after the initial analysis of the structural brain scans, participant S01, has been excluded due to her injury being considerably more severe than other participants. All the final analyses in this paper have been performed on a cohort of 13 participants. Additionally, 13 sex- and age-matched controls underwent the structural and functional neuroimaging protocols but did not complete Dutton's questionnaire. The controls were recruited through local advertisement and convenience sampling.

Materials

Data collection spanned three modalities: behavioral assessment, neuroimaging, and structural/functional visual diagnostics. Data collection was performed between 2021 and 2024. Behavioral evaluation of patients' functional impairments relied on a 15-items scale adapted into Swedish and chosen from the broader clinical inventory developed by Gordon Dutton (Cerebral Visual Impairment Assessment, 2023). Because the original inventory was designed as a descriptive catalog of daily visual challenges rather than a validated screening tool, it lacks a standardized quantitative scoring system. Selection of questions focused on items capturing daily functional activities which can be most strongly related to respectively distinct ventral (e.g., object and face recognition) and dorsal stream operations (e.g., spatial orientation and visuomotor integration).

Each question was completed by the participant and a parent answering together, using a binary response format ("ja" / "nej") to indicate the presence or absence of a given difficulty in daily life, alongside dedicated space for extra comments. In collaboration with the supervising ophthalmologist, each item was categorized as predominantly driven by either ventral stream function (7 items) or dorsal stream function (8 items), see Table 1.

Table 1.

Study Materials Assessing Dorsal and Ventral Visual Processing Functions in Children

Administered Questions	English Translation	Visual Function	Processing Stream Categorization
1. "Känna igen personer/ansikten"	Recognizing people's faces	Recognition	Ventral
2. "Känna igen personer på fotografier"	Recognizing people in photographs	Recognition	Ventral
3. "Känna igen former, föremål"	Recognizing shapes, objects	Recognition	Ventral
4." Hitta hemma"	Orientation at home	Orientation	Dorsal
5. "Hitta i skolan, på dagis"	Orientation in school/preschool	Orientation	Dorsal
6. Orientera sig i nya omgivningar	Orientation in new surroundings	Orientation	Dorsal
7. Bedöma avstånd och höjdskillnader	Judging distances and height differences	Spatial & Motion Processing	Dorsal
8. Se föremål som rör sig	See objects that are moving	Spatial & Motion Processing	Dorsal
9. Se föremål när barnet själv är i rörelse/t.ex åker bil	See objects when the child is moving themselves / e.g. riding in a car	Spatial & Motion Processing	Dorsal
10. Hitta föremål på en mönstrad matta	Identifying objects on a carpet	Pattern recognition	Ventral
11. Hitta föremål i komplicerade bilder	Identifying objects in a complex image	Pattern recognition	Ventral

12. Rita	Drawing	Visuomotor integration	Dorsal
13. Lägga pussel	Doing puzzles	Visuomotor integration	Dorsal
14. Se tecknade filmer	Watching cartoons	Visual Media Processing	Ventral
15. Läsa serietidningar	Reading comic books	Visual Media Processing	Ventral

Complementary structural and functional visual metrics were acquired using Optical Coherence Tomography (OCT) to measure retinal layer integrity, alongside automated visual field perimeter to map visual field sensitivity. All the OCT data was acquired via Topcon Apparatus.

Neuroimaging was performed at the National 7T facility at Lund University Bioimaging Center (LBIC), Lund University, using a 32-channel head coil. High-resolution structural imaging was acquired using a 3D T1-weighted MP2RAGE sequence (0.7-mm isotropic resolution). For brain lesion assessment, 3D FLAIR-images were acquired. pRF fMRI was acquired using T2*-weighted single-shot EPI (2-mm isotropic resolution, 56 slices, TR/TE = 1500/25 ms, SENSE 3, multiband factor 2) during presentation of a high-contrast sliding-bar stimulus traversing the visual field in eight directions, illustrated in Figure 4. The paradigm comprised 136 stimulus frames, including blank periods, corresponding to the 136-volume functional run, following the pRF mapping approach of Dumoulin and Wandell (2008). Structural data were processed using the study-specific "7T_anatprep" pipeline (Phillips, n.d.-a), including MP2RAGE reconstruction, denoising, tissue segmentation and FreeSurfer cortical surface reconstruction. The repository describes subsequent fMRIPrep processing in native surface space. Functional data were processed using the "7T_funcproc" pipeline (Phillips, n.d.-b), operating on fMRIPrep output and using *pybest* for functional denoising and *prfpy* for pRF model fitting. pRF modelling generated estimates of receptive-field position and size and cortical representations of polar angle and eccentricity. For regional analysis, the probabilistic retinotopic atlas of Wang et al. (2015) was transformed from standard space to each participant's native anatomy. Separate dorsal and ventral subdivisions of early visual areas in each hemisphere (e.g., V1d/V1v, V2d/V2v and V3d/V3v) were used to extract pRF characteristics, enabling quadrant-wise analysis of the upper and lower portions of the left and right visual hemifields.

Figure 4.

Sliding Bar Stimulus Utilized in the Study

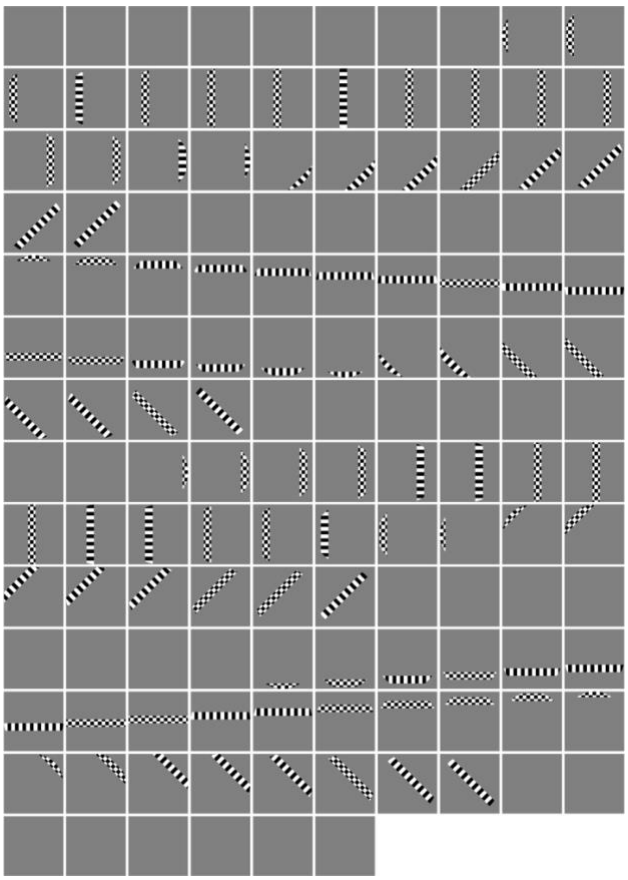

Procedure

Institutional Review and Ethical Clearance

This study has been conducted under the ethical permission Dnr 2020-06677 granted by the Swedish Ethical Review Authority (*Etikprövningsmyndigheten*). Sensitive, medical data was collected and handled in accordance with the Swedish Data Protection Authority's (*Integritetsskyddsmyndigheten*) Security Standards.

Data Acquisition

All data acquisition occurred at the 7-Tesla MRI facility at Lund Bioimaging Centre (LBIC), Lund University/Skåne University Hospital. Participants travelled to the facility with their accompanying guardian, on two separate occasions. During the first experimental session they underwent the OCT scanning and filled-out Dutton's questionnaire. The second session was dedicated purely for the scanning procedure. The experimental sessions for each participant and control were administered in the span of 1-3 weeks.

The paper-based Swedish adaptation of the Dutton questionnaire was administered on-site during the testing session. Each participant completed the inventory in collaboration with a parent or legal guardian. The questionnaires were scored jointly by the researcher and the supervising ophthalmologist.

Although initial responses were recorded binarily ("ja"/"nej"), final categorization incorporated the accompanying qualitative comments to resolve discrepancies: a "no" response was re-categorized as "yes" if written comments indicated that the functional problem occurred in daily life (or vice versa). Furthermore, if a problem was reported by either party, for instance, if the parent noted a difficulty in the comments while the child answered "no", it was categorized as "yes."

Retinal layer integrity metrics, specifically GLC+, were extracted digitally from OCT scan outputs. Visual field sensitivity maps were exported from automated static perimeter files. For the functional, tier-2 analysis, raw ultra-high-field 7T fMRI data were retrieved from the central imaging database. Functional data underwent standard preprocessing pipelines using ITK-SNAP (*ITK-SNAP Home*, n.d.), and custom 7T functional workflows, including denoising algorithms and pRF estimation mapping utilizing an 8-bar visual display matrix. To account for ultra-high-field tissue boundary missegmentation, structural MRI volumes underwent manual mask refinement in ITK-SNAP using a standardized protocol (brush size: 2 voxels, opacity: 50%). Processing followed a three-step workflow: *Step 1:* Mapping and isolating the sagittal sinus within the occipital cortex, initially located in the sagittal plane and subsequently adjusted in the axial (horizontal) view. *Step 2:* Removing non-brain tissue inclusions, specifically dural "bleeding" artifacts. *Step 3:* Manually adding omitted neural tissue to ensure complete coverage of the cerebral cortex, cerebellum, and brainstem.

Data Quality Control

Quality control criteria were applied across all three modalities prior to the analysis. OCT scans were evaluated for signal intensity and layer segmentation accuracy. Scans with a signal strength below 40db or significant motion artifacts were excluded. Visual field perimetry files were checked for fixation reliability, which was assessed by the perimetrist administering the data collection. 7T structural scans were evaluated across multiple quality indicators: anatprep completion, sagittal sinus delineation, dural artifact removal, cortical coverage integrity, overall image quality (granulation, shimming, and movement artifacts), FreeSurfer surface reconstruction validity, and preprocessing run completion. Tier 2 analysis inclusion criteria were based on quality matrix evaluations and consistency across radiology, OCT, and visual perimetry. A subset of four participant cases (S06, S08, S09, and S14) met all technical criteria: adequate shimming, minimal motion degradation, successful pRF mapping, and sufficient, cross-domain alignment.

Analysis

Tier 1

Dutton's Questionnaire Analysis

To characterize individual profiles of visual processing dysfunction across the ventral and dorsal streams, I implemented a double-dissociation score-matching procedure. Given the constraints of standard

parametric latent variable modeling in small samples, this non-parametric spatial approach maps each participant's relative impairment bias across the two functional pathways. Because the questionnaire has an asymmetric item distribution (8 dorsal vs. 7 ventral items) and contained one missing value on question 11, calculating pure raw scores could not be used. For each participant, I computed the stream-specific impairment scores as the proportion of "yes" responses relative to the total number of valid (non-missing) items completed within that specific stream.

$$Ventral\ Score_i = \frac{\Sigma_{j=1}^{kv,i} V_{ij}}{k_{v,i}},\ Dorsal\ Score_i = \frac{\Sigma_{m=1}^{kv,i} D_{im}}{k_{d,i}}$$

Note. Ventral Score$_i$ and Dorsal Score$_i$ indicate the stream-specific impairment proportions for participant i. V_{ij} and D_{im} denote the binary response (1 = impaired, 0 = unimpaired) of participant i to ventral item j and dorsal item m, respectively. $k_{v,i}$ and $k_{d,i}$ represent the total number of valid, non-missing items completed by participant i within the ventral (maximum = 7) and dorsal (maximum = 8) subscales. $\sum$ indicates the summation across completed items indexed by j and m.

To evaluate functional asymmetries, individual proportion scores were mapped onto a two-dimensional Cartesian coordinate system (X = Ventral Score, Y= Dorsal Score). An identity line of parity (y = x) was defined as the theoretical baseline representing equal proportional impairment across both processing pathways. Deviation from balanced impairment was operationalized as the orthogonal distance from each participant's coordinate on the identity line:

$$Stream\ Bias_i = \frac{y_i - x_i}{\sqrt{2}}$$

Note. $Stream\ Bias_i$ represents the orthogonal distance from each participant's coordinate to the identity line ($y = x$) on a two-dimensional Cartesian coordinate system. Specifically, y = Ventral Score, x = Dorsal Score, and i = individual participant.

A positive value (stream bias > 0) would indicate a dorsal-dominant impairment bias. A negative value (stream Bias < 0) indicated a Ventral-dominant impairment bias. Values approaching zero represented symmetrical deficits across both streams. The magnitude of the orthogonal segment ({Stream Biasi}) shows the degree of functional dissociation, independently of total global impairment severity. High-severity symmetrical profiles (1.0, 1.0) and low-severity symmetrical profiles (0.25, 0.25) both anchored on the line of parity, allow for differentiation between total visual impairment load and stream-specific dissociation.

To test the construct validity of mapping questionnaire items onto a theoretical, top-down visual streams classification, a dual-dendrogram Hierarchical Cluster Analysis (HCA) Dual-Dendrogram Heatmap Visualization was conducted using the *pheatmap* package in R, was implemented as a data-driven, bottom-up validation strategy. Calculating complete-linkage item clusters from participant response profiles. The clustering aimed to evaluate whether these items naturally co-occur along pathway lines in a

clinical CVI cohort. Dissimilarity between binary response profiles (0 = nej / no impairment,1 = ja / impairment) across both rows (participants) and columns (Dutton's items) was estimated using Euclidean distance. Clustering of items was performed via complete linkage, which defines inter-cluster distance as the maximum distance between any single object in the first cluster and any single object in the second cluster. This method creates compact clusters, preventing the chaining effects common to single-linkage clustering.

Structural and Functional Visual Field Analysis

Firstly, the average, combined GCL+ thickness was compared between the participant and the control group via the independent sample t-test, to see if the patient's cohort generally does exhibit significant thinning. Ona a dyad level, the percentage, the thickness changes among each participant versus control can be seen in Appendix 1. Secondly, to determine whether local structural thinning aligns spatially with functional visual field loss, an intra-eye quadrant analysis was performed separately for structural (GCL+) and functional (VF) metrics for each participant. For a given eye, I calculated mean values across the four quadrants. The quadrant with the minimum degradation was defined as the primary reference quadrant. Delta scores were derived by subtracting each remaining quadrant's mean from the reference quadrant. The quadrant generating the maximum delta score was designated as the target eye's worst quadrant. Spatial concordance was performed as a direct topological match between the worst quadrant identified in retinal thickness metric and the worst quadrant identified in visual field metric. Importantly, the comparison had to account for the anatomical transformation between the spatial alignment of the retina versus the visual field, as *superior nasal & inferior temporal*, *superior temporal & inferior nasal*. Results are presented via bivariate spatial plots mapping structural and functional defect overlays.

Lastly, to evaluate regional structural thinning while controlling for visual field eccentricity, retinal thickness values (μm) across four anatomical quadrants: Upper-Left (UL), Upper-Right (UR), Lower-Left (LL), and Lower-Right (LR). Mean thickness values were computed across eccentricity bins extending from the central region (0.8 grid units) to the periphery (5.6 grid units). Control data were composed to generate mean thickness profiles (±1SD) across all eccentricity bins per quadrant, against which individual patient profiles were evaluated. To test for significant localized structural loss, group differences between patients and controls were assessed across spatial bins using independent-samples t-tests. Benjamini-Hochberg False Discovery Rate (FDR) corrections were applied to adjust for multiple comparisons across the spatial bins, with adjusted $p<0.05$ considered statistically significant.

Structural MRI Analysis

To further evaluate downstream visual pathway integrity, a second-tier neuroimaging analysis was conducted on a selected sub-cohort of participants (N=4) who demonstrated minimal head motion, and sufficient functional signal-to-noise ratios during their scans. Structural T1-weighted neuroimaging scans

were processed to evaluate cortical structure, occipital gray matter volume, and localized structural visual cortex lesions among the CVI participants. T1 structural volumes were processed using automated cortical surface reconstruction pipelines (e.g., FreeSurfer) to generate inflated and flattened cortical surface maps of the occipital pole. Scans were evaluated for structural abnormalities, including sulcal enlargement, focal cortical thinning, or white matter alterations along the optic radiations and primary visual pathway structures (V1, V2, V3). Qualitative and morphometric cortical damage findings were compared to each participant's GCL+ thinning profiles to assess whether primary visual cortex structural degradation corresponded spatially with localized retinal pathology.

To characterize functional visual cortex alterations, pRF mapping was conducted using functional MRI retinotopic stimulation paradigms. For each voxel within retinotopically defined visual areas (V1, V2, V3, and ventral/dorsal sub-regions), a standard two-dimensional Gaussian pRF model was fitted. The model estimated the receptive field center location (x, y) and its spatial size (defined as the standard deviation of the 2D Gaussian profile). Because pRF size scales with visual field eccentricity, individual voxel-wise pRF sizes were modeled as a function of eccentricity (in degrees of visual angle) separately for each visual area.Individual participant pRF size-versus-eccentricity functions were evaluated against an age-matched controls. Deviation from normative control ranges was evaluated to test for enlarged pRF sizes, quantifying functional cortical reorganization or loss of spatial tuning sharpness across visual areas.

Tier 2

pRF Analysis

Population receptive fields parameters for each voxel were estimated using a standard two-dimensional (2D) isotropic Gaussian model (Dumoulin & Wandell, 2008) implemented in the prfpy Python framework. For every functional voxel, the model fits a 2D Gaussian profile defined by spatial visual field coordinates (x,y) and a spatial tuning width parameter (σ, representing pRF size). The model time-course prediction is generated by convolving the stimulus aperture design matrix (representing the moving bar positions across time) with the participants 2D Gaussian function, followed by convolution with a hemodynamic response function (HRF). Model parameters (x,y,σ) are optimized to minimize the residual sum of squares between predicted and observed BOLD signals, with goodness-of-fit quantified by R^2. Rather than projecting functional data onto reconstructed cortical surface meshes, pRF fitting was performed directly in volumetric functional space on 2mm isotropic voxels. This volumetric fitting bypasses dependencies on individual cortical surface reconstruction quality, which can be compromised by structural brain lesions or ventricular enlargement, and eliminates spatial interpolation steps, minimizing the loss of functional information. To identify the boundaries of visual areas in each participant's brain, the probabilistic visual topographic atlas developed by Wang et al. (2015), which identifies 25 retinotopic visual areas in each hemisphere, was transformed into each participant's individual anatomical space. Non-

linear transformation matrices generated during fMRIPrep preprocessing were applied to warp the MNI-space Wang atlas to each participant's space and resampled directly onto the exact voxel grid of the functional BOLD data. This atlas explicitly divides early visual areas (V1, V2, V3) into ventral (V1v, V2v, V3v) and dorsal (V1d, V2d, V3d) sub-regions, enabling stream-specific comparisons across visual hierarchies.

Results

Dutton's Questionnaire Analysis

The double-dissociation score-matching analysis revealed heterogeneity in visual stream impairment profiles among the clinical participants. Mapping proportional dorsal and ventral scores relative to the line of parity ($y=x$) differentiated overall deficit severity from stream-specific functional asymmetries, as shown in Figure 5. Participants P5, P6, P7, P8, P9, P10, P11, and P12 exhibited dorsal-dominant impairment profiles reflecting proportionally higher spatial, motion, and visuomotor deficits relative to object and pattern recognition impairments. Participants P5 and P6 demonstrated the strongest dorsal-dominant dissociation (Dorsal = 0.71, Ventral = 0.13), positioned farthest below the parity line, followed by P11 and P12 (Dorsal = 0.86, Ventral = 0.38). Conversely, participants P2, P4, P13, and P14 displayed ventral-dominant impairment profiles, indicating disproportionate deficits in ventral-mediated functions such as face, object, and detail recognition. Participant P14 showed the strongest ventral-dominant dissociation (Ventral = 0.88, Dorsal = 0.14), positioned farthest above the parity line. Participant P3 fell directly on the line of parity (grey marker; Dorsal = 1.00, Ventral = 1.00), representing a balanced profile characterized by maximal, global impairment across both functional visual pathways.

Figure 5.

Double-Dissociation of Dorsal Versus Ventral Stream Impairment Profiles

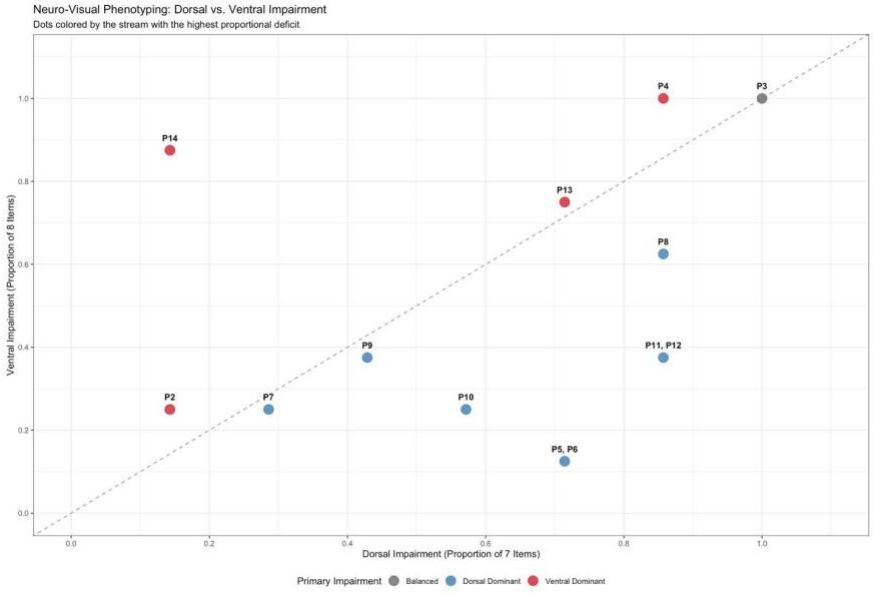

Note. Participant proportional impairment scores mapped relative to the theoretical line of parity (y = x). Dotted vectors represent the orthogonal deviation (Stream Bias) from equal impairment. Positive values (red/orange) indicate a dorsal-dominant impairment asymmetry, whereas negative values (blue/green) indicate a ventral-dominant asymmetry.

The column dendrogram identified two main item clusters of the functional visual domain taxonomy, see Figure 3. Items probing movement perception (*Se föremål som rör sig*), self-motion (*Se föremål när barnet själv är i rörelse*), spatial judgment (*Bedöma avstånd och höjdskillnader*), visual search (*Hitta föremål i komplicerade bilder*), and orientation (*Orientera sig i nya omgivningar*) clustered together. Impairments reported in these items were prevalent across most participant profiles. Tasks requiring visual pattern discrimination and fine detail processing, such as face recognition (*Känna igen personer ansikten/fotografier*), form recognition (*Känna igen former/föremål*), and media reading (*Läsa serietidningar*, *Se tecknade filmer*), formed a secondary cluster. Deficits in this cluster showed selective sparing in dorsal-dominant participants (e.g., P9, P11). Participants P3 and P14 (and to a close extent P2 and P13) formed a cluster characterized by impairments across both dorsal and ventral item clusters. Participants P4, P8, P11, P5, P7, and P10 formed an intermediate cluster marked impairments of spatial and motion perception items, alongside variable sparing of facial and visual media recognition. Participants P9 and P12 clustered together, displaying sparse deficits restricted to isolated visual functions (e.g., visual media or specific spatial tasks) while demonstrating preserved functioning across object-recognition items.

Figure 6.

Dual-Dendrogram Heatmap Visualization of Tested Items

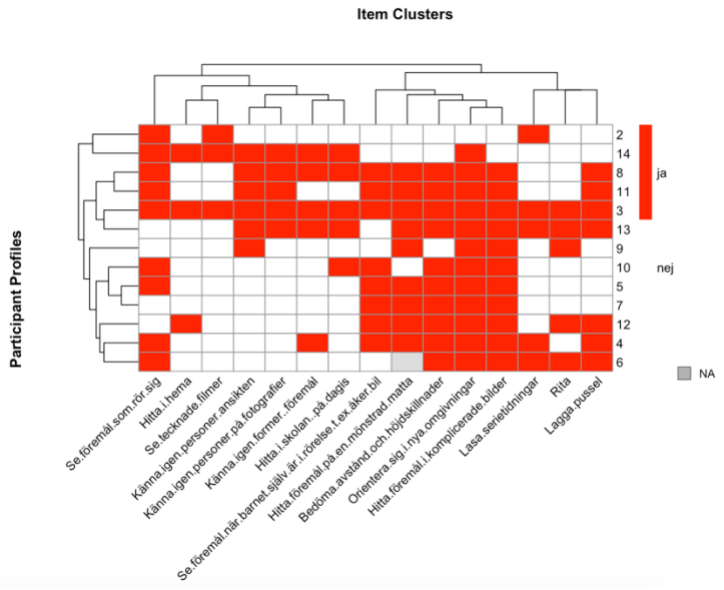

Structural and Functional Visual Field Analysis

To examine the retinal integrity, a global mean GCL+ score (μm) was calculated for everyone by averaging layer thickness measurements across all eight quadrants of both eyes. A Welch's two-sample t-test was conducted to compare global GCL+ thickness between the participant cohort (n = 14) and healthy controls (n = 14). The analysis revealed a statistically significant (p <0.01) reduction in overall GCL+ thickness among the participants ($\bar{x}$ = 60.10µm, SD = 4.41µm) compared to the control group ($\bar{x}$= 67.43µm, SD = 5.25µm)

To assess how GCL+ thinning relates to functional visual field defects across individuals, participants (N = 14) were categorized by their overall spatial concordance profile: Bilateral Concordance (both eyes exhibiting direct spatial matching), Unilateral Concordance (spatial matching restricted to a single eye), or No Concordance (spatial decoupling across evaluated eyes). The detailed results of the quadrant concordance can be seen in Table 2 and presented visually in Figure 4. Only a single participant (S14) demonstrated bilateral structure-function concordance, where the worst structural retinal quadrant accurately predicted the corresponding optically inverted functional visual field defect in both the right and left eyes. Six participants (S03, S06, S08, S09, S10, S13) displayed unilateral concordance. Half of the participant cohort (S01, S02, S04, S05, S11, S12, and S13's OD) exhibited no spatial concordance in any valid, evaluated eye. In these individuals, the location of maximal retinal thinning did not correspond topographically to the region of greatest visual field sensitivity loss.

Table 2.

Participant-Level Categorization of Spatial Structure-Function Concordance Between GCL+ Thinning and Visual Field Defects

Concordance Category	Participant Count (N)	Percentage (%)
Bilateral Concordance	1	7.6%
Unilateral Concordance	6	46.2%
No Concordance	6	46.2%
Total Cohort	13	100%

Note. N = 13. Spatial concordance indicates direct topological agreement between the worst-performing ganglion cell layer (GCL+) quadrant and the corresponding optically inverted total threshold visual field sector. Percentages reflect proportions relative to the total participant cohort. S12 OD was excluded prior to classification due to incomplete perimetric visual field data.

Figure 7.

Quadrant-Level Structure-Function Concordance Between Retinal Thickness and Visual Field Defect

Note. OD = right eye; OS = left eye.

To evaluate structural retinal thinning while accounting for visual field eccentricity, OCT radial thickness profiles (*μm*) were evaluated across four retinal quadrants (Upper-Left, UL; Upper-Right, UR; Lower-Left, LL; Lower-Right, LR) as a function of eccentricity from the grid center, which can be seen in Figure 7. Patients demonstrated consistent mean structural thinning relative to the control mean across all eccentricity bins, with the most pronounced separation observed in the upper quadrants (UL and UR). In quadrant UL, control mean thickness peaked near 88μm at 2.4 units eccentricity before tapering to 48μm peripherally, whereas patient mean thickness reached a maximum of 72μm across central eccentricities before declining to 46μm. Similarly, in quadrant UR, patient thickness profiles remained suppressed across central and mid-peripheral bins compared to controls. In contrast, lower quadrants (LL and LR) showed smaller mean differences between groups, though individual patient profiles displayed inter-individual variability, with several patients falling well below 1 SD of the control reference band.

Figure 8.

Retinal Thickness Profiles Across Retinal Quadrants as a Function of Eccentricity Across Dyads

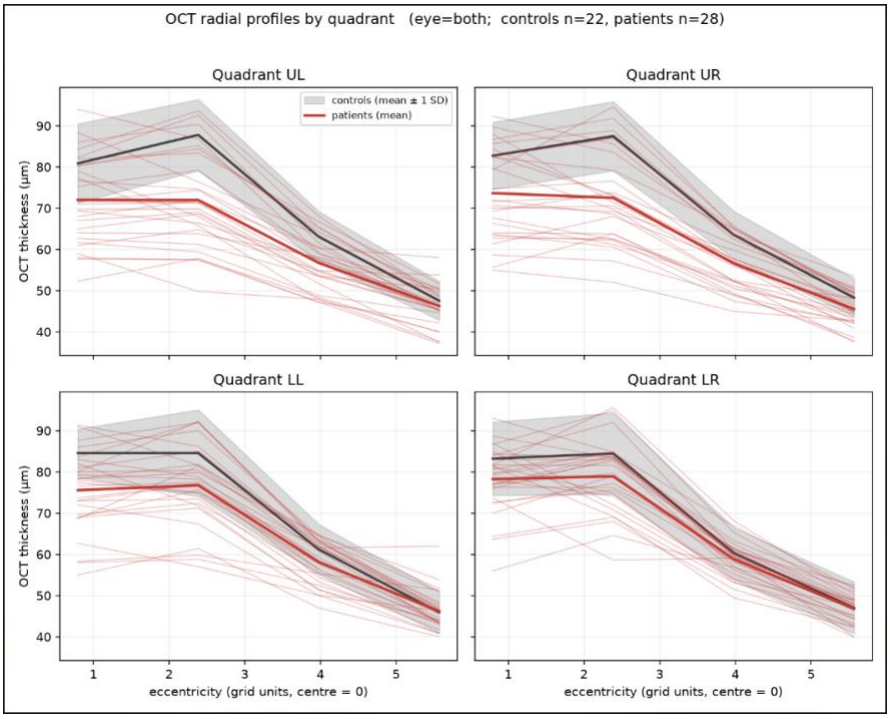

Structural MRI Findings

Qualitative evaluation of high-resolution 7-Tesla structural MRI (FLAIR and MP2RAGE) revealed a spectrum of structural abnormalities across the participant cohort ($N = 14$). Periventricular leukomalacia (PVL) was the predominant neurostructural pathology, identified in 10 of the 14 subjects. The specific structural brain profiles per subject are presented in Table 3. Manifestations of PVL ranged from slight periventricular white matter (WM) reduction to extensive bilateral volume loss (e.g., S07 and S09). WM volume loss was consistently localized to parieto-occipital regions, particularly within the periventricular areas surrounding the trigones and posterior horns of the lateral ventricles. Non-PVL structural focal lesions were noted in S02, who showed localized loss of brain tissue accompanied by gliosis[3] in the right occipital region, resulting from a prior neonatal hemorrhage. S01 presented with generalized WM loss, particular parietal regions, secondary ventricular dilatation, periventricular gliosis, and bilateral thalamic volume reduction. Two subjects exhibited near-normal structural neuroanatomy: S04 showed no significant

[3] is the central nervous system's reactive scarring response to injury or disease, characterized by the proliferation and enlargement of glial cells (mainly astrocytes).

structural abnormalities, while S11 demonstrated only mild, isolated thinning of the posterior region of corpus callosum.

Structural damage of the optic radiations (OR) was identified in 12 of the 14 participants based on the location of their brain lesions. Eight participants (S01, S03, S07, S08, S09, S10, S12, S14) showed bilateral OR damage, although the extent of it was often uneven between the two sides and was frequently more pronounced in the superior parts of the OR. Three participants showed unilateral OR involvement: S02 had right sided OR damage, while S05 and S13 had focal areas of gliosis mainly affecting the left OR. Three participants (S04, S06, S11) showed no structural abnormalities in the OR.

Secondary thinning of the corpus callosum was identified in 11 subjects (S01, S03, S05, S06, S07, S08, S09, S11, S12, S13, S14), predominantly affecting the posterior segments of the callosal body. Severe callosal thinning was observed in S01 and S07.

Table 3

Individual Structural 7T MRI Results

Subject	Brain Structure Presentation	Optic Radiation Presentation	Corpus Callosum Presentation	MRI Scan
S02	Right occipital parenchymal loss and gliosis (neonatal hemorrhage)	Unilateral (Right)	Normal	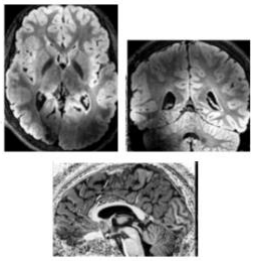
S03	Mild-to-moderate bilateral PVL, periventricular gliosis	Bilateral (Left > Right)	Mild thinning of the isthmus	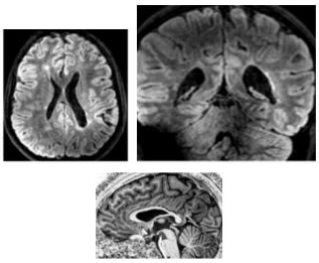

S04	Normal	Normal	Normal	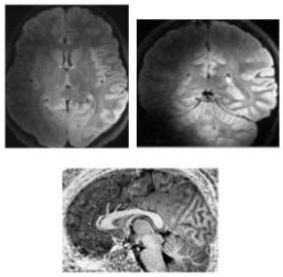
S05	Mild bilateral PVL, asymmetric posterior ventricular enlargement	Unilateral (Left)	Mild thinning of the isthmus	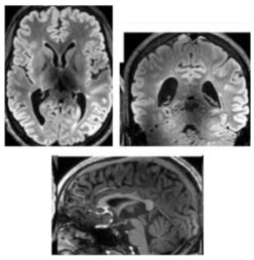
S06	Subtle PVL, mild parietal WM reduction	Normal	Mild thinning of the splenium	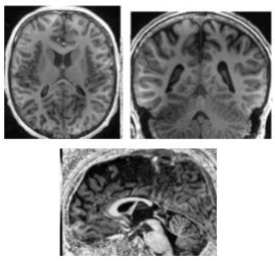
S07	Severe PVL, parietal/frontal WM loss, gliosis, periventricular cysts	Bilateral (Left > Right, superior focus)	Diffuse thinning (body/isthmus)	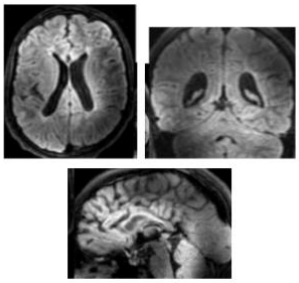

S08	PVL, posterior horn gliosis, cella media/anterior horn WM changes	Bilateral (Left > Right, superior focus)	Subtle thinning of the body	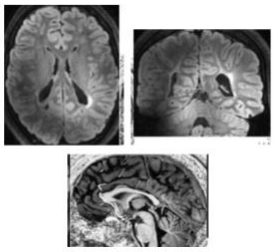
S09	PVL, periventricular WM reduction, cystic changes cranial to trigones	Bilateral (Superior focus)	Thinning of the posterior portion	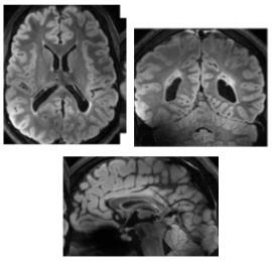
S10	Bilateral symmetric PVL, parieto-central gliosis in centrum semiovale	Bilateral (Left > Right)	Normal	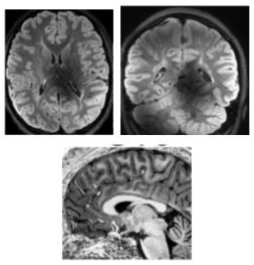
S11	Isolated minor callosal variation	Normal	Mild thinning of the isthmus	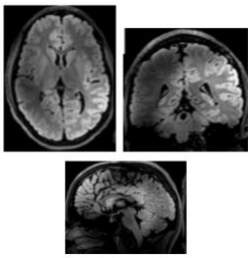
S12	PVL, posterior/trigonal WM loss, secondary ventricular dilatation	Bilateral	Thinning of the body and isthmus	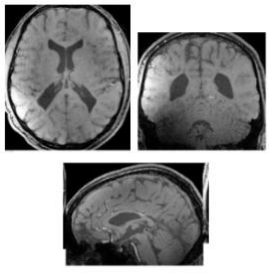

S13	PVL, posterior WM loss, patchy gliosis left posterior horn	Unilateral (Left)	Normal	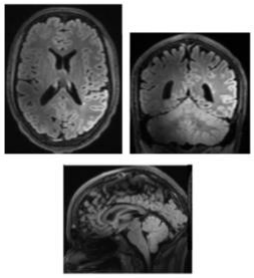
S14	PVL, trigonal WM loss, secondary ventricular dilatation, gliosis	Bilateral (Superior focus)	Minor thinning of the isthmus	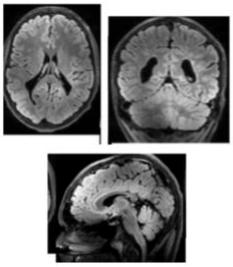

Population Receptive Fields Analysis

Within-subject descriptive analyses were conducted to evaluate visual field coverage, eccentricity-dependent coverage variations, and spatial retinotopic alignment across all functional voxels. Subject S07 exhibited poor signal quality, generating an insufficient amount of suprathreshold voxels (n = 99, compared to n ≈ 550 in remaining subjects) hence dyad 7 was excluded from all descriptive interpretations. Finally, only dyad 14 has been evaluated. For each subject, visual field parameters were visualized using two diagnostic plots *(_prf.png and _benson.png*). Visual field coverage maps (_prf.png), which can be viewed in Appendix 2, depict the spatial density and extent of fitted population pRF centers across the 5.4° visual field. To quantify spatial coverage independent of global, subject-level signal-to-noise ratio (SNR), a normalized, quadrant coverage index was computed. For each visual quadrant, mapped to contralateral dorsal and ventral sub-streams (V1–V3), the proportion of functional voxels producing measurable pRFs was scaled relative to the subject's mean voxel yield across the visual field (where 1.0 indicates perfectly uniform coverage):

$$Coverage\ Index_{quadrant} = \frac{Voxel\ Fraction_{quadrant}}{Mean\ Subject\ Voxel\ Fraction}$$

Horizontal quadrant indices were used to measure hemifield coverage symmetry. Vertical quadrant indices exhibited systematic baseline offsets across subjects, including opposing bias directions in control datasets, which could be attributed to differential cortical depth mask coverage and eccentricity sampling

ranges across ventral and dorsal cortices. Partitioning coverage into within-subject central (light) and peripheral (dark) eccentricity quantiles revealed distinct spatial profiles. Notably, Subject S08 demonstrated severe peripheral coverage depletion (dark band coverage indices ranging from 0.35 to 0.42 across all quadrants) alongside intact central coverage (light band coverage indices ranging from 1.20 to 1.70). Across all evaluated subjects, pRF size demonstrated a positive, monotonic relationship with visual field eccentricity, confirming that parameter estimation preserved expected physiological scaling properties. Visual spatial alignment (_benson.png) was evaluated by computing voxel-wise polar angle error, defined as the difference between pRF polar angle estimates and anatomically predicted polar angles derived from the Benson et al. (2014) structural template:

$$\Delta\theta_{voxel} = \theta_{measured} - \theta_{predicted}$$

Eccentricity predictions were excluded from error calculations due to a constant +0.5° to +1.7° visual angle offset observed across subjects, reflecting a calibration difference between template space and the 5.4°visual display. Kernel density estimates of voxel-wise angular error ($\Delta\theta$) were centered on 0° across all visual quadrants. Median absolute angular error (MAE) ranged between 14° and 23° across quadrants, tracking localized variance in model fit quality (R^2). No systematic angular shifts or quadrant-specific polar displacements were observed in any subject. Surviving cortical population receptive fields remained anchored to their anatomically predicted retinotopic coordinates. This preservation of spatial alignment suggests that visual field defects in early retro-geniculate injury reflect localized loss of measurable cortical responsiveness (functional deafferentation) rather than spatial remapping or topological displacement of surviving visual cortical fields.

Discussion

Characterizing CVI requires a unified, empirical framework that bridges structural pathology, cortical reorganization, and real-world visual cognition. Due to its multimodal nature, the diagnostic process is difficult and time and resource consuming. Children affected by CVI benefit from receiving the diagnosis early so that they can begin necessary therapeutic activities and that their family and school environment can be maximally tailored to their needs. In this study, I aimed at gaining more insight in the combining OCT, visual field perimetry, fMRI pRF mapping, and dual-stream questionnaires, to determine how retino-cortical degeneration and cortical neuroplasticity converge to shape individual clinical phenotypes. Addressing Research Question 1, whether regional retinal loss predicts cortical spatial neuroplasticity, the hypothesis that macular ganglion cell layer (GCL+) thinning relates to enlarged early visual pRF sizes received no direct, dyad-specific support. In the Tier 2 analysis, participant S14 exhibited elevated primary visual cortex (V1) pRF sizes relative to age-matched control C14 while maintaining monotonic eccentricity scaling, accompanied by bilateral structural brain damage and behavioral

impairments as measured by the Dutton's scale. However, the observed pattern diverged from initial theoretical expectations. To evaluate such neurophysiological alterations, it is essential to establish clear theoretical boundaries distinguishing adaptive functional compensation from maladaptive reorganization and passive neural alterations driven by atypical visual input.

From a computational standpoint, an increase in estimated pRF size (σ) reflects an expansion in the spatial extent of neural pooling across visual space (Haak et al., 2012; Elul & Levin, 2024). While broader spatial integration may serve an adaptive compensatory function by pooling degraded visual signals across damaged receptive fields to preserve signal-to-noise ratios, several alternative neurophysiological mechanisms ought to be considered. First, pRF enlargement may represent a maladaptive loss of local GABAergic, intracortical inhibition (Dinkin, 2017). Structural injury to retro-geniculate pathways or hypoxic-ischemic damage can selectively compromise vulnerable inhibitory mechanisms in cortical layers II/III and IV, causing receptive fields of adjacent excitatory pyramidal neurons to expand passively due to unconstrained lateral excitation (Dinkin, 2017; Lennartsson et al., 2018). Rather than enhancing visual processing, this disinhibition degrades spatial acuity and elevates visual crowding. Second, pRF expansion may stem from a loss of top-down feedback from higher-order extrastriate areas (e.g., V2, V3, MT/V5), which normally exert inhibitory spatial constraint over V1 (Haak et al., 2012). Third, from a methodological perspective, pRF estimates are highly sensitive to fixational instability, micro-saccades, and retinal slip, common occurrences in pediatric CVI cohorts. Uncorrected eye movements during bar-pass stimulus presentations broaden the spatial envelope of blood-oxygen-level-dependent (BOLD) signal fluctuations across time, which forward-modeling algorithms fit as an expanded Gaussian profile. Thus, while broadened neural pooling in S14 may tentatively compensate for dorsal stream loss at the expense of ventral resolution, the possibility that observed pRF expansion reflects passive disinhibition, or fixational noise does not allow for definitive conclusions regarding adaptive reorganization.

An important finding of this investigation was the lack of spatial concordance between macular GCL+ thinning and perimetric visual field defects across the CVI cohort. Contrary to the hypothesis predicting that localized retinal degeneration would map spatially onto visual field scotomas, structure–function dissociations were widespread. This spatial dissociation can be explained through several physiological and methodological frameworks. Methodologically, resolution and coordinate disparities between diagnostic instruments posed a major barrier in this study. Macular OCT provides a continuous metric of cellular thickness across a fine grid, whereas static automated perimetry measures differential light sensitivity exponentially in decibels across discrete test locations. Furthermore, standard grid comparisons often fail to incorporate mathematical displacement models that account for the radial displacement of foveal retinal ganglion cell (RGC) bodies relative to their overlying photoreceptors

(Lennartsson et al., 2021). Physiologically, this lack of concordance could align with the concept of pre-perimetric degeneration. Due to structural redundancy in the human macula, up to 30--50% of RGCs or their axons can degenerate before luminance detection thresholds on perimetry drop below normal population variability. Conversely, localized visual field scotomas may originate from focal subcortical or striate lesions where retrograde trans-synaptic degeneration has not yet fully manifested in the retina, given the prolonged and variable temporal kinetics of trans-synaptic RGC apoptosis (Dinkin, 2017; Lennartsson et al., 2018).

Regarding Research Question 2, whether individuals display a dorsal-dominant visual dysfunction that tracks overall pRF expansion, the hypothesis was only partially supported. Interpreting these behavioral outcomes requires grounding them within the classical dual-stream cognitive framework formulated by Goodale and Milner (1992) and Mishkin et al. (1983). The dorsal pathway functions as a "vision-for-action" system dedicated to spatial awareness, visually guided motor control, motion processing, and visual scene navigation (Chokron & Dutton, 2016; Cooper & O'Sullivan, 2016). Clinical dysfunction in this stream manifests as optic ataxia, impaired distance judgment, visual crowding, and simultanagnosia (Dutton et al., 2006; Macintyre-Beon et al., 2010). In contrast, the ventral pathway serves a "vision-for-perception" role, mediating object recognition, face processing, and form-from-color analysis (Kravitz et al., 2013). In alignment with established literature on Dorsal Stream Vulnerability (DSV) in CVI (Bennett et al., 2020; Macintyre-Beon et al., 2010), dorsal stream dysfunction was the modal phenotype (61.54%, $n = 8$) on the Swedish adaptation of Dutton's Questionnaire, and hierarchical clustering confirmed functional stream independence. However, distinct ventral-dominant (28.6%, $n = 4$) and globally impaired (7.1%, $n = 1$) profiles also emerged. This distribution indicates that V1 pRF enlargement does not operate as a linear predictor of overall deficit load but may instead act as a functional moderator of pathway asymmetry (Pamir et al., 2024).

Evaluating Research Question 3, whether structural, computational, and behavioral metrics converge to reveal a developmental structure–function dissociation, the hypothesis predicting that pRF expansion mitigates structural damage to selectively reduce dorsal deficits received only partial support. In cases of severe subcortical white matter injury (Volpe et al., 2011) without early cortical pRF expansion, participants presented with severe, unmitigated global deficits (e.g., P3: Dorsal = 1.00, Ventral = 1.00). Conversely, in dyad S14, early visual V1 pRF expansion was associated with a selective rescue of dorsal spatial "vision-for-action" functions despite extensive structural damage, shifting the clinical presentation toward lower-than-expected dorsal deficits and a relative ventral-dominant asymmetry (S14/P14: Dorsal = 0.14, Ventral = 0.88). However, an important alternative explanation for the preservation of dorsal spatial abilities in the presence of severe geniculostriate or V1 damage is the functional operation of subcortical visual pathways, specifically the tectopulvinar pathway. This pathway

projects directly from retinal ganglion cells to the superior colliculus and pulvinar nucleus, bypassing V1 entirely to target motion-sensitive extrastriate area MT/V5 and posterior parietal regions. In children with early cortical injury, spatial orientation and visually guided action can be sustained via this subcortical route. Thus, preserved dorsal functionality in S14 may be mediated by subcortical visual rescue rather than cortical V1 pRF reorganization. Demonstrating true functional compensation requires evidence that altered central neural organization actively mitigates expected behavioral deficits relative to the severity of underlying anatomical injury, which should be conducted via longitudinal study where one CVI patient can be evaluated at different points in time in order to assess the extend and directionality of neurological re-organization, separated from the mere results of the initial injury.

Limitations and Future Directions

Several methodological limitations must be acknowledged. First, despite holding official diagnoses of CVI, the participant cohort exhibited marked structural heterogeneity. Participants S04, S06, and S11 demonstrated minimal to no observable cortical damage on structural MRI and negligible retinal thinning relative to controls (with S04 and S06 even displaying relative retinal "thickening"). Yet, all three reported pronounced real-world visual difficulties on Dutton's Questionnaire. Cross-sectional comparison of GCL+ thickness against neurotypical controls is prone to Type II errors, as pathological thinning in an individual with naturally thick baseline retinas will be masked when compared against population averages. Future studies should implement longitudinal, within-subject designs that track localized retino-cortical metrics over time. Second, limitations surrounding the administration and classification of Dutton's Questionnaire remain. Parent-report inventories are susceptible to observational biases and can be confounded by co-occurring motor impersistence, visual spatial neglect, or executive dysfunction. Furthermore, ongoing debate regarding the classification of inventory items into rigid dorsal vs. ventral categories underscores the need for expanded, standardized behavioral instruments (such as multi-item Swedish inventories; Hellgren et al., 2020) and rigorous top-down and bottom-up validation studies (Farivar et al., 2009; Sakki et al., 2021; St Clair Tracy et al., 2025).

In conclusion, these findings demonstrate that CVI is defined by intricate structure–function relations, wherein central cortical adaptations like pRF expansion operate semi-independently of retino-structural degeneration. Single-modality diagnostic metrics used in isolation lack the capacity to capture the full spectrum of developmental visual dysfunction. Differentiating true adaptive plasticity from passive neural alterations, subcortical path preservation, and methodological artifacts will be crucial to refining multimodal diagnostic frameworks and designing targeted habilitation programs for young patients with CVI.

References

Bennett, C. R., Bauer, C. M., Bailin, E. S., & Merabet, L. B. (2020). Neuroplasticity in cerebral visual impairment (CVI): Assessing functional vision and the neurophysiological correlates of dorsal stream dysfunction. *Neuroscience & Biobehavioral Reviews*, *108*, 171–181. https://doi.org/10.1016/j.neubiorev.2019.10.011

Cerebral Visual Impairment Assessment. (2023, July 28). https://www.ulster.ac.uk/research/topic/biomedical-sciences/research/optometry-and-vision-science/vision-resources/professionals/cerebral-visual-impairment-assessment

Chang, M. Y., Merabet, L. B., Borchert, M., Chandna, A., Heidary, G., Kran, B., Lawrence, L., Legge, R. H., Lehman, S., Rice, M., Shah, V., Stasheff, S., Chen, D., Cruz, T., Goetz, K., Gordon, S., Hardy, K., Kerr, A., Nelson, E., … Wiggs, C. (2024). Special Commentary: Cerebral/Cortical Visual Impairment Working Definition: A Report from the National Institutes of Health CVI Workshop. *Ophthalmology*, *131*(12), 1359–1365. https://doi.org/10.1016/j.ophtha.2024.09.017

Chokron, S., & Dutton, G. N. (2016). Impact of Cerebral Visual Impairments on Motor Skills: Implications for Developmental Coordination Disorders. *Frontiers in Psychology*, *7*. https://doi.org/10.3389/fpsyg.2016.01471

Cooper, S. A., & O'Sullivan, M. (2016). Here, there and everywhere: Higher visual function and the dorsal visual stream. *Practical Neurology*, *16*(3), 176–183. https://doi.org/10.1136/practneurol-2015-001168

Dinkin, M. (2017). Trans-synaptic Retrograde Degeneration in the Human Visual System: Slow, Silent, and Real. *Current Neurology and Neuroscience Reports*, *17*(2). https://doi.org/10.1007/s11910-017-0725-2

Dumoulin, S. O., & Wandell, B. A. (2008). Population receptive field estimates in human visual cortex. *NeuroImage*, *39*(2), 647–660. https://doi.org/10.1016/j.neuroimage.2007.09.034

Dutton, G. N. (2009). "Dorsal stream dysfunction" and "dorsal stream dysfunction plus": A potential classification for perceptual visual impairment in the context of cerebral visual impairment? *Developmental Medicine and Child Neurology*, *51*(3), 170–172. https://doi.org/10.1111/j.1469-8749.2008.03257.x

Dutton, G. N. (2011). Structured history taking to characterize visual dysfunction and plan optimal habilitation for children with cerebral visual impairment. *Developmental Medicine & Child Neurology*, *53*(5), 390–390. https://doi.org/10.1111/j.1469-8749.2010.03900.x

Dutton, G. N., McKillop, E. C. A., & Saidkasimova, S. (2006). Visual problems as a result of brain damage in children. *British Journal of Ophthalmology*, *90*(8), 932–933. https://doi.org/10.1136/bjo.2006.095349

Elul, D., & Levin, N. (2024). The Role of Population Receptive Field Sizes in Higher-Order Visual Dysfunction. *Current Neurology and Neuroscience Reports*, *24*(12), 611–620. https://doi.org/10.1007/s11910-024-01375-6

Farivar, R., Blanke, O., & Chaudhuri, A. (2009). Dorsal–Ventral Integration in the Recognition of Motion-Defined Unfamiliar Faces. *The Journal of Neuroscience*, *29*(16), 5336–5342. https://doi.org/10.1523/JNEUROSCI.4978-08.2009

Fazzi, E., Bova, S., Giovenzana, A., Signorini, S., Uggetti, C., & Bianchi, P. (2009). Cognitive visual dysfunctions in preterm children with periventricular leukomalacia. *Developmental Medicine & Child Neurology*, *51*(12), 974–981. https://doi.org/10.1111/j.1469-8749.2009.03272.x

Good, W. V., Jan, J. E., DeSa, L., Barkovich, A. J., Groenveld, M., & Hoyt, C. R. eig S. (1994). Cortical visual impairment in children. *Survey of Ophthalmology*, *38*(4), 351–364. https://doi.org/10.1016/0039-6257(94)90073-6

Goodale, M. A., & Milner, A. D. (1992). Separate visual pathways for perception and action. *Trends in Neurosciences*, *15*(1), 20–25. https://doi.org/10.1016/0166-2236(92)90344-8

Haak, K. V., Cornelissen, F. W., & Morland, A. B. (2012). Population Receptive Field Dynamics in Human Visual Cortex. *PLoS ONE*, *7*(5), e37686. https://doi.org/10.1371/journal.pone.0037686

Hellgren, K., Jacobson, L., Frumento, P., Bolk, J., Ådén, U., Libertus, M. E., & Benassi, M. (2020). Cerebral visual impairment captured with a structured history inventory in extremely preterm born children aged 6.5 years. *Journal of AAPOS: The Official Publication of the American Association for Pediatric Ophthalmology and Strabismus*, *24*(1), 28.e1-28.e8. https://doi.org/10.1016/j.jaapos.2019.11.011

Kooiker, M. J. G., Pel, J. J. M., van der Steen-Kant, S. P., & van der Steen, J. (2016). A Method to Quantify Visual Information Processing in Children Using Eye Tracking. *Journal of Visualized Experiments: JoVE*, (113), 54031. https://doi.org/10.3791/54031

Kravitz, D. J., Saleem, K. S., Baker, C. I., Ungerleider, L. G., & Mishkin, M. (2013). The ventral visual pathway: An expanded neural framework for the processing of object quality. *Trends in Cognitive Sciences*, *17*(1), 26–49. https://doi.org/10.1016/j.tics.2012.10.011

Lennartsson, F., Nilsson, M., Flodmark, O., Jacobson, L., & Larsson, J. (2018). Injuries to the Immature Optic Radiation Show Correlated Thinning of the Macular Ganglion Cell Layer. *Frontiers in Neurology*, *9*. https://doi.org/10.3389/fneur.2018.00321

Lennartsson, F., Öhnell, H., Jacobson, L., & Nilsson, M. (2021). Pre- and Postnatal Damage to the Retro-Geniculate Visual Pathways Cause Retinal Degeneration Predictive for Visual Function. *Frontiers in Human Neuroscience*, *15*, 734193. https://doi.org/10.3389/fnhum.2021.734193

Macintyre-Beon, C., Ibrahim, H., Hay, I., Cockburn, D., Calvert, J., N. Dutton, G., & Bowman, R. (2010). Dorsal Stream Dysfunction in Children. A Review and an Approach to Diagnosis and Management. *Current Pediatric Reviews*, *6*(3), 166–182. https://doi.org/10.2174/157339610793743895

Martín, M. B. C., Santos-Lozano, A., Martín-Hernández, J., López-Miguel, A., Maldonado, M., Baladrón, C., Bauer, C. M., & Merabet, L. B. (2016). Cerebral versus Ocular Visual Impairment: The Impact on Developmental Neuroplasticity. *Frontiers in Psychology*, *7*. https://doi.org/10.3389/fpsyg.2016.01958

McKillop, E., & Dutton, G. N. (2008). Impairment of vision in children due to damage to the brain: A practical approach. *British and Irish Orthoptic Journal*, *5*(0). https://doi.org/10.22599/bioj.222

Mishkin, M., Ungerleider, L. G., & Macko, K. A. (1983). Object vision and spatial vision: Two cortical pathways. *Trends in Neurosciences*, *6*, 414–417. https://doi.org/10.1016/0166-2236(83)90190-X

Mitry, D., Bunce, C., Wormald, R., & Bowman, R. (2013). Childhood visual impairment in England: A rising trend. *Archives of Disease in Childhood*, *98*(5), 378–380. https://doi.org/10.1136/archdischild-2012-301970

Ospina, L. H. (2009). Cortical Visual Impairment. *Pediatrics In Review*, *30*(11), e81–e90. https://doi.org/10.1542/pir.30.11.e81

Pamir, Z., Manley, C. E., Bauer, C. M., Bex, P. J., Dilks, D. D., & Merabet, L. B. (2024). Visuospatial processing in early brain-based visual impairment is associated with differential recruitment of dorsal and ventral visual streams. *Cerebral Cortex*, *34*(5), bhae203. https://doi.org/10.1093/cercor/bhae203

Philip, S. S., & Dutton, G. N. (2014). Identifying and characterising cerebral visual impairment in children: A review. *Clinical & Experimental Optometry*, *97*(3), 196–208. https://doi.org/10.1111/cxo.12155

Ribeiro, F. L., Benson, N. C., & Puckett, A. M. (2025). Human retinotopic mapping: From empirical to computational models of retinotopy. *Journal of Vision*, *25*(8), 14. https://doi.org/10.1167/jov.25.8.14

Sakki, H., Bowman, R., Sargent, J., Kukadia, R., & Dale, N. (2021). Visual function subtyping in children with early-onset cerebral visual impairment. *Developmental Medicine and Child Neurology*, *63*(3), 303–312. https://doi.org/10.1111/dmcn.14710

St Clair Tracy, H., McDowell, N., Dutton, G. N., Ravenscroft, J., Hay, I., & Blaikie, A. (2025). Emulation of the subjective experience of visual dorsal stream dysfunction: A description of three in depth case studies. *Frontiers in Human Neuroscience*, *18*, 1496811. https://doi.org/10.3389/fnhum.2024.1496811

Tierney, A. L., & Nelson, C. A. (2009). Brain Development and the Role of Experience in the Early Years. *Zero to Three*, *30*(2), 9–13.

Volpe, J. J., Kinney, H. C., Jensen, F. E., & Rosenberg, P. A. (2011). The developing oligodendrocyte: Key cellular target in brain injury in the premature infant. *International Journal of Developmental Neuroscience: The Official Journal of the International Society for Developmental Neuroscience*, *29*(4), 423–440. https://doi.org/10.1016/j.ijdevneu.2011.02.012

Appendix 1

GCL+ thickness dynamics across individual dyads

PERCENTAGE THICKNESS LOSS

Dyad	OD/upper/Left	OD/upper/right	OD/lower/left	OD/lower/right	OS/upper/left	OS/upper/right	OS/lower/left	OS/lower/right
2	13.08	6.84	19.38	4.84	15.33	7.57	17.02	8.62
3	17.67	17.12	20.46	16.74	20.57	18.31	17.88	12.33
4	-9.77	-3.28	-12.17	-12.40	-6.47	-8.67	-10.64	-10.03
5	20.43	14.67	16.89	18.21	22.16	14.10	19.67	20.36
6	-18.58	-23.73	-20.99	-24.38	-25.09	-23.25	-27.36	-32.49
7	13.07	22.56	13.63	8.56	-2.55	4.22	-15.12	-17.40
8	11.76	18.60	2.95	8.95	13.79	16.59	5.10	7.34
9	24.47	18.94	-2.02	6.48	7.40	14.99	9.48	8.08
10	16.35	27.50	11.49	0.72	15.44	17.69	6.93	0.34
11	-35.85	-44.39	-22.85	-2.83	12.80	8.42	12.02	9.01
12	14.27	20.52	NA	2.69	18.58	19.28	0.42	3.67
13	16.32	11.94	9.45	9.36	18.75	10.43	9.97	12.68
14	8.27	26.85	14.05	5.89	28.19	11.80	13.25	7.16

Thinning classification	
Negligible	< 5%
Moderate	5-20%
Severe	>20%

"Thickening" classification	
Negligible	< 5%
Moderate	5-20%
Severe	>20%

Appendix 2

pRF analysis plots and figures of dyad 7 and dyad 14

Dyad 7

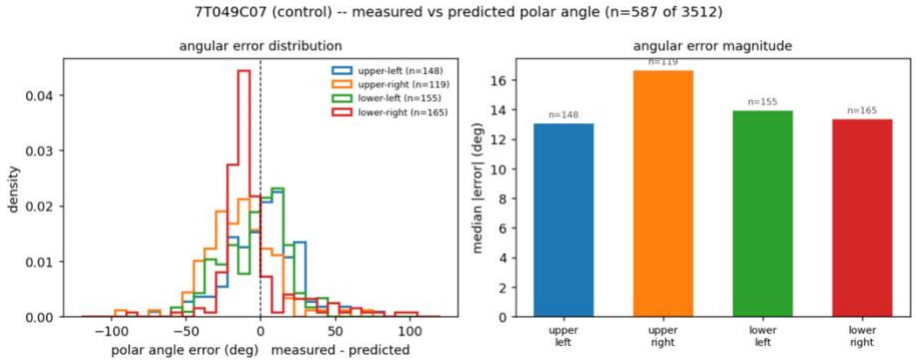

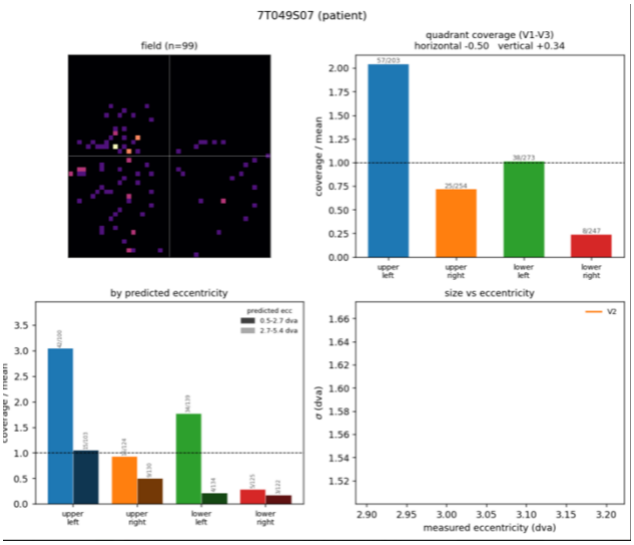

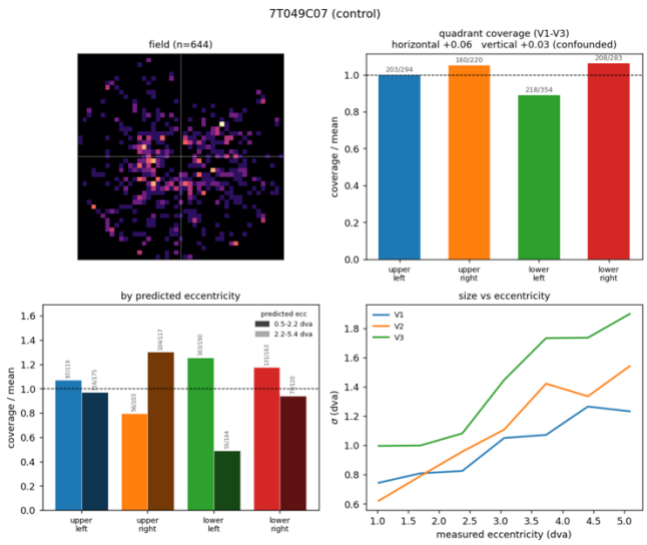

Dyad 14

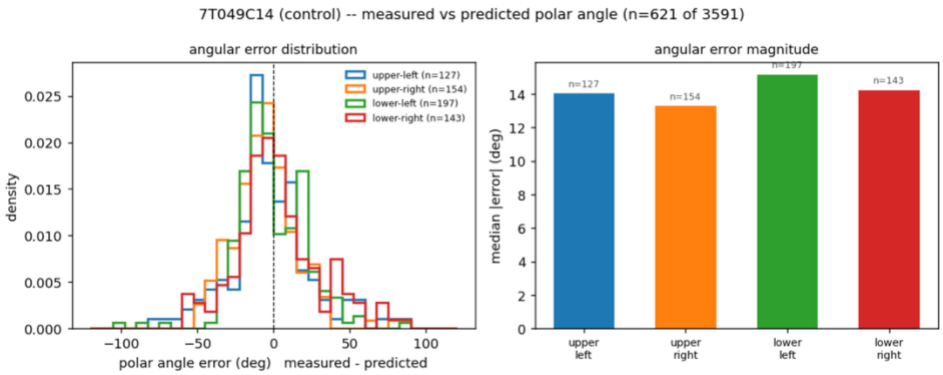
7T049C14 (control) -- measured vs predicted polar angle (n=621 of 3591)
angular error distribution
upper-left (n=127)
upper-right (n=154)
lower-left (n=197)
lower-right (n=143)
density
polar angle error (deg) measured - predicted
angular error magnitude
median |error| (deg)
n=127
n=154
n=197
n=143
upper left
upper right
lower left
lower right

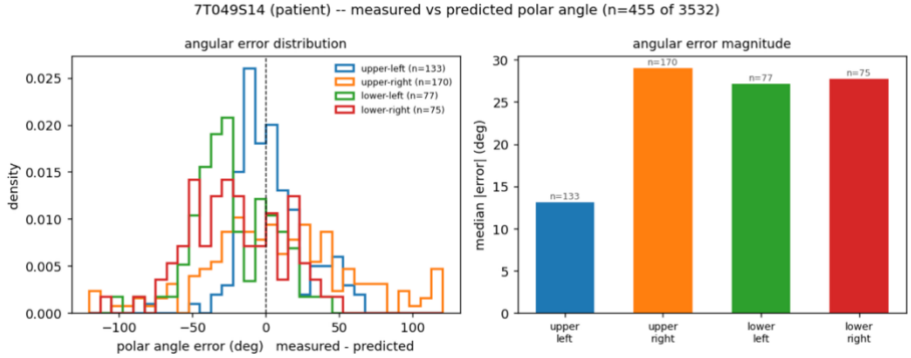
7T049S14 (patient) -- measured vs predicted polar angle (n=455 of 3532)
angular error distribution
upper-left (n=133)
upper-right (n=170)
lower-left (n=77)
lower-right (n=75)
density
polar angle error (deg) measured - predicted
angular error magnitude
median |error| (deg)
n=133
n=170
n=77
n=75
upper left
upper right
lower left
lower right

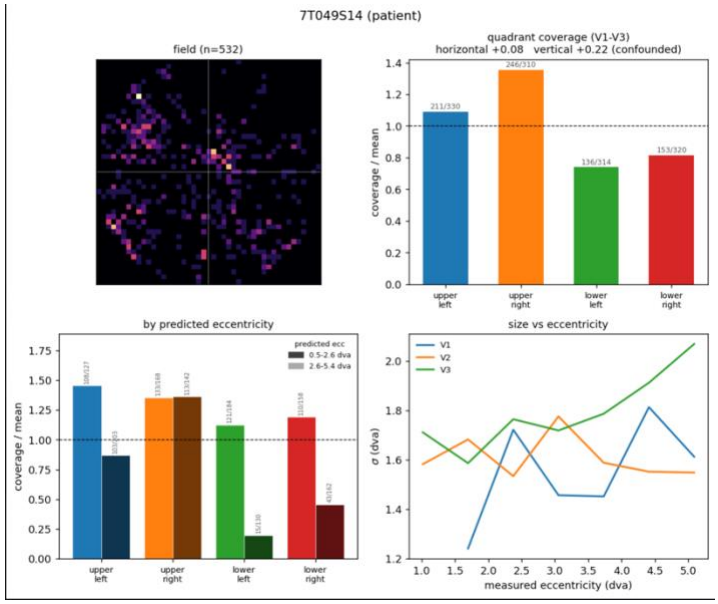
7T049S14 (patient)
field (n=532)
quadrant coverage (V1-V3)
horizontal +0.08 vertical +0.22 (confounded)
coverage / mean
211/330
246/310
136/314
153/320
upper left
upper right
lower left
lower right
by predicted eccentricity
predicted ecc
0.5-2.6 dva
2.6-5.4 dva
size vs eccentricity
V1
V2
V3
σ (dva)
measured eccentricity (dva)

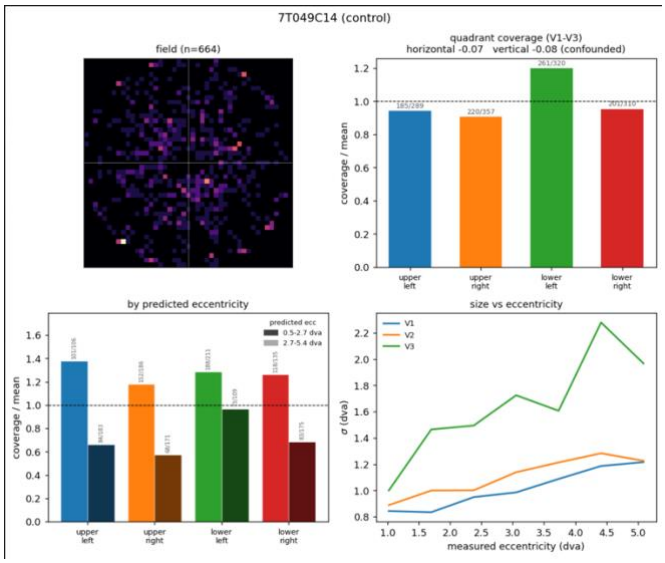
7T049C14 (control)
field (n=664)
quadrant coverage (V1-V3)
horizontal -0.07 vertical -0.08 (confounded)
coverage / mean
upper left
upper right
lower left
lower right
by predicted eccentricity
predicted ecc
0.5-2.7 dva
2.7-5.4 dva
size vs eccentricity
V1
V2
V3
σ (dva)
measured eccentricity (dva)